

Available online at www.sciencedirect.com

SciVerse ScienceDirect

journal homepage: www.JournalofSurgicalResearch.com

Three-dimensional quantitative ultrasound for detecting lymph node metastases

Emi Saegusa-Becroft, MD,^{a,b,*} Junji Machi, MD, PhD, FACS,^a Jonathan Mamou, PhD,^c Masaki Hata, MD, PhD,^d Alain Coron, PhD,^{e,f} Eugene T. Yanagihara, MD, FCAP,^b Tadashi Yamaguchi, PhD,^g Michael L. Oelze, PhD,^h Pascal Laugier, PhD,^{e,f} and Ernest J. Feleppa, PhD, FAIUM, FAIMBE^c

^a Department of Surgery, University of Hawaii and Kuakini Medical Center, Honolulu, Hawaii

^b Department of Pathology, Kuakini Medical Center, Honolulu, Hawaii

^c Lizzi Center for Biomedical Engineering, Riverside Research, New York, New York

^d Department of Surgery, Juntendo University, School of Medicine, Tokyo, Japan

^e University Pierre and Marie Curie, Université Paris 06, Paris, France

^f Centre National de la Recherche Scientifique, Laboratoire d'Imagerie Paramétrique, Paris, France

^g Research Center for Frontier Medical Engineering, Chiba University, Chiba, Japan

^h Department of Electrical and Computer Engineering, University of Illinois, Urbana, Illinois

ARTICLE INFO

Article history:

Received 9 October 2012

Received in revised form

12 November 2012

Accepted 7 December 2012

Available online 8 January 2013

Keywords:

Three-dimensional quantitative ultrasound

High-frequency ultrasound

Lymph node metastases

Lymph node micrometastases

Breast cancer

Colorectal cancer

Gastric cancer

Prospective cohort study

Step-sectioning histology

ABSTRACT

Purpose: Detection of metastases in lymph nodes (LNs) is critical for cancer management. Conventional histological methods may miss metastatic foci. To date, no practical means of evaluating the entire LN volume exists. The aim of this study was to develop fast, reliable, operator-independent, high-frequency, quantitative ultrasound (QUS) methods for evaluating LNs over their entire volume to effectively detect LN metastases.

Methods: We scanned freshly excised LNs at 26 MHz and digitally acquired echo-signal data over the entire three-dimensional (3D) volume. A total of 146 LNs of colorectal, 26 LNs of gastric, and 118 LNs of breast cancer patients were enrolled. We step-sectioned LNs at 50- μ m intervals and later compared them with 13 QUS estimates associated with tissue microstructure. Linear-discriminant analysis classified LNs as metastatic or nonmetastatic, and we computed areas (A_z) under receiver-operator characteristic curves to assess classification performance. The QUS estimates and cancer probability values derived from discriminant analysis were depicted in 3D images for comparison with 3D histology.

Results: Of 146 LNs of colorectal cancer patients, 23 were metastatic; $A_z = 0.952 \pm 0.021$ (95% confidence interval [CI]: 0.911–0.993); sensitivity = 91.3% (specificity = 87.0%); and sensitivity = 100% (specificity = 67.5%). Of 26 LNs of gastric cancer patients, five were metastatic; $A_z = 0.962 \pm 0.039$ (95% CI: 0.807–1.000); sensitivity = 100% (specificity = 95.3%). A total of 17 of 118 LNs of breast cancer patients were metastatic; $A_z = 0.833 \pm 0.047$ (95% CI: 0.741–0.926); sensitivity = 88.2% (specificity = 62.5%); sensitivity = 100% (specificity = 50.5%). 3D cancer probability images showed good correlation with 3D histology.

Conclusions: These results suggest that operator- and system-independent QUS methods allow reliable entire-volume LN evaluation for detecting metastases. 3D cancer probability

Presented at the American College of Surgeons' 97th Annual Clinical Congress, San Francisco, CA, October 2011.

* Corresponding author. Department of General Surgery, University of Hawaii and Kuakini Medical Center, 405 N. Kuakini Street, Suite 601, Honolulu, HI 96817. Tel.: +1 808 440 2250; fax: +1 808 596 0370.

E-mail address: esaegusa@hawaii.edu (E. Saegusa-Becroft).

0022-4804/\$ – see front matter © 2013 Elsevier Inc. All rights reserved.

<http://dx.doi.org/10.1016/j.jss.2012.12.017>

images can help pathologists identify metastatic foci that could be missed using conventional methods.

© 2013 Elsevier Inc. All rights reserved.

1. Introduction

For many cancers, accurate detection of metastases in lymph nodes (LNs) is crucial to determine the disease stage using the American Joint Committee on Cancer tumor-node-metastases staging system. Changes in the node status affect treatment and management. The latest edition categorizes micrometastases (0.2–2 mm) and isolated tumor cells (<0.2 mm or <1000 tumor cells) separately from macrometastases. Micrometastases are considered to be clinically significant and positive for metastases [1].

For all cancers, pathologists currently perform a microscopic histologic examination of surgically dissected LNs. For colorectal cancer and gastric cancer, only one central histological section of each LN is usually evaluated for metastases, regardless of LN size [2,3]. For invasive carcinoma of the breast, the College of American Pathologists recommends that each LN should be sliced parallel to the long axis of the LN at a spacing of 2 mm. These slices are then submitted for microscopic examination with at least one representative hematoxylin and eosin (H&E)-stained thin section obtained from the surface of each slice examined histologically [4].

To date, no method is clinically available for examining LNs in their entire volume to detect metastases. Molecular studies such as reverse transcription polymerase chain reaction have been reported [5–8], but continue to be a research topic and have not been adopted for clinical practice. There is some consensus in the literature that treatment decisions should not yet be based on these techniques [1–4,9–12]. The reference standard remains histologic examination of H&E histology, and occasionally additional sections from the specimen may be required for subsequent special staining, such as immunohistochemical methods [4,13,14]. With the conventional method, unless the metastases are included in the section examined microscopically, metastases, particularly micrometastases, may be missed [15–22].

Breast sentinel LN biopsy now is well established in the United States for clinically node-negative axillas [9,23]. Touch-prep imprinting and frozen-section procedures for detection of metastases provide limited sensitivity because of sampling limitations [9,24–28]. Multiple-level step sectioning of specimens has been reported to detect more metastases [15–18,20–22]. Different countries and facilities have reported their own protocols for multilevel step-sectioning at different intervals of axillary sentinel LNs of breast cancer patients [4,29–31], but to date, no international consensus on an optimal histopathology procedure exists [31]. The clinical impact on the outcome of detecting occult micrometastases and isolated tumor cells remains controversial [4,17,21,32–35]. Recently, the need to complete a formal axillary LN dissection in patients with a positive sentinel LN biopsy showing macrometastases or micrometastases in fewer than three nodes has been questioned [36] and remains controversial [37]. However, many of these studies do not account for the

potential true residual disease prevalence in axillary LNs, because metastases are detected using limited conventional histopathologic procedures. If a new method could be developed to rapidly assess LNs for suspicion of metastases non-invasively over the entire LN volume before histology processing, the new method would resolve the current controversies and would have broad implications for staging a wide range of cancers.

The aim of our study was to develop a fast, reliable, and operator-independent method for entire-volume LN examination to detect and image LN metastases using high-frequency (HF) quantitative ultrasound (QUS) [38,39]. By using HF ultrasound (i.e., >15 MHz) and digitally acquiring and analyzing the ultrasound echo signals, QUS methods can provide estimates of tissue microstructure on a subresolution scale. Unlike B-mode ultrasound images currently used clinically, QUS methods are operator independent and provide a quantitative means of estimating microscopic-scale tissue properties. These attributes, combined with the ability of three-dimensional (3D) ultrasound scans to acquire data from the full LN volume, enable QUS methods to evaluate the entire LN and detect micrometastases as well as macrometastases. Future clinical 3D QUS systems potentially will enable surgeons and pathologists to detect metastatic LNs with high sensitivity.

2. Materials and methods

2.1. Enrollment

A total of 160 patients (44 men and 116 women) with histologically proven colorectal, gastric, and breast cancer, who underwent cancer surgery at the Kuakini Medical Center in Honolulu, Hawaii, were randomly and consecutively enrolled in this prospective study. This patient cohort included 71 patients (all women) with breast cancer, 77 patients (38 men and 39 women) with colorectal cancer, and 12 patients with gastric cancer (6 men and 6 women). The median age for each cancer type was: breast, 65 y (range, 42–93 y; mean, 67.4 y; standard deviation [SD], 12.5 y); colorectal, 74 y (range, 40–95 y; mean, 71 y; SD, 13.1 y); and gastric, 81.5 y (range, 52–93 y; mean, 76.3 y; SD, 14.1 y).

Institutional review boards at the University of Hawaii and the Kuakini Medical Center approved the study protocol. We obtained written informed consent from all patients.

2.2. Materials

Study materials were LNs harvested from surgical specimens dissected from previously untreated patients with histologically proven colorectal, gastric, or breast cancer; axillary sentinel LNs that underwent an imprint (i.e., “touch-prep”) cytology procedure satisfied this criterion. The study excluded

Table – Classification performance.									
Cancer type	Patients	Total LNs	Metastatic LNs	Benign LNs	Area under ROC curve	95% Confidence interval	Effective QUS estimates	Sensitivity	Specificity
Colorectal	77	146	23	123	0.952 ± 0.021	0.911–0.993	4 (Scatter size, Nakagami α , quantile-quantile Sa, quantile-quantile Cy)	100.00%	67.50%
Gastric	12	26	5	21	0.962 ± 0.039	0.807–1.000	3 (Scatter size, intercept, Homodyned-K k)	91.30%	87.00%
Breast	71	118	17	101	0.833 ± 0.047	0.741–0.926	4 (Scatter size, slope, quantile-quantile Cy, Homodyned- K μ)	100.00%	50.50%
								88.20%	62.50%

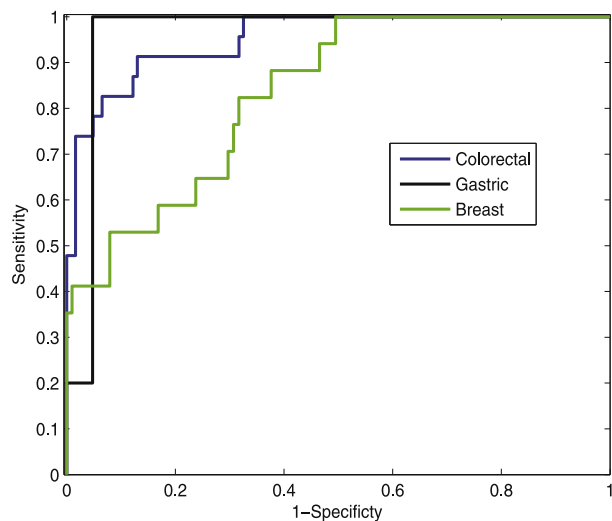


Fig. 1 – ROC curves for LNs of the three cancer types. Blue line, colorectal cancer; black line, gastric cancer; green line, breast cancer. The ROC curves indicate superior classification performance for colorectal and gastric cancers compared with breast cancer. ROC = receiver-operator characteristic.

LNs with undetermined primary cancer origins, LNs undergoing a frozen-section procedure because of potential tissue damage, large LNs that did not fit in the standard embedding cassette (3.0 × 2.6 cm), and LNs that were retrieved after formalin fixation or immersion in fat-clearing solutions.

We harvested LNs from freshly excised gross surgical specimens submitted to pathology for standard of care histologic evaluation. We carefully removed excess perinodal adipose tissue during the LN harvest, leaving 0.3–0.5 mm of surrounding fat layer to avoid inadvertently removing lymphoid tissue. The study procedures did not interfere with the standard of care pathology protocol, but added histologic information by microscopically examining each LN over its entire volume by step-sectioning, instead of using conventional methods, which only examine thin sections obtained from the central plane of the node or from 2-mm-thick sections.

The investigator was independent of the surgical and the pathology service and did not have access to clinical information. The investigator performing the dissections was informed only that the LNs were dissected from histologically proven colorectal, and gastric, and breast cancer patients, and was blinded from clinical information such as clinical presentation, history, physical examination, palpable LN status, primary tumor properties such as histologic type, size, grade, and so forth. Freshly excised LNs were randomly selected from the gross surgical specimen and were immediately submerged in 0.9% normal saline, pinned to a sound-absorbing material, and then scanned with HF ultrasound to acquire radiofrequency (RF) echo-signal data.

2.3. High-frequency ultrasonic data acquisition

We designed a custom, HF ultrasound, laboratory scanning system and built it to acquire RF echo-signal data in 3D from

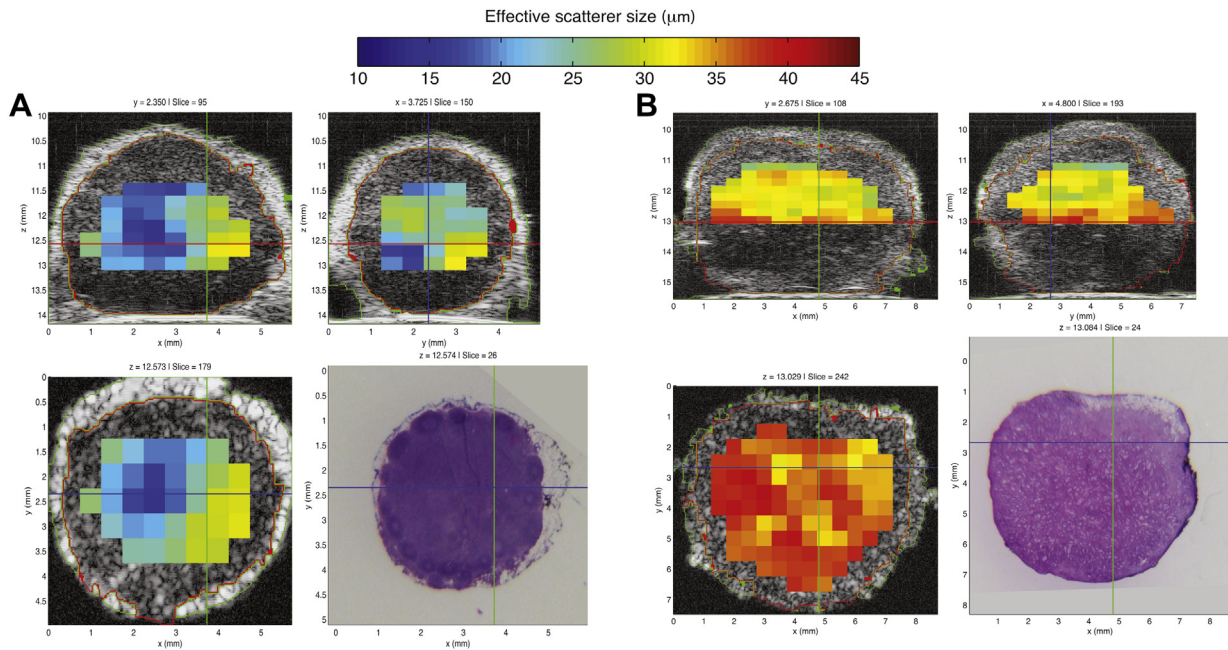


Fig. 2 – Illustrative QUS images: 3D cross-sectional parametric images displaying effective scatter-size estimates. (A) 3D cross-sectional parametric images of a benign locoregional LN from a colon cancer patient. (B) 3D cross-sectional parametric images of a locoregional LN with diffusely metastatic adenocarcinoma from a different colon cancer patient. Parametric cross-sectional B-mode images are shown with overlaid color-coded effective scatter-size estimates. Bottom right panel of each figure displays the co-registered histology of the bottom left panel. (Color version of figure is available online.)

freshly excised LNs. This system allowed LNs to be scanned over their entire volume. The scanning apparatus featured a single-element, spherically focused, ultrasound transducer (PI-30; Olympus NDT, Waltham, MA) with a 12.2-mm focal length and 6.1-mm aperture. The transducer had a center frequency of 25.6 MHz and a -6 -dB bandwidth that extended

from 16.4 to 33.6 MHz. We digitized the received RF echo signals at a 400-MHz sampling frequency with an accuracy of 8 bits. Scan vectors were uniformly spaced by 25 μm in X and Y directions across the entire scan volume to acquire complete full-volume 3D data from each LN [38,39]. Typical scanning time ranged from 5 to 30 min, depending on the size of the LN.

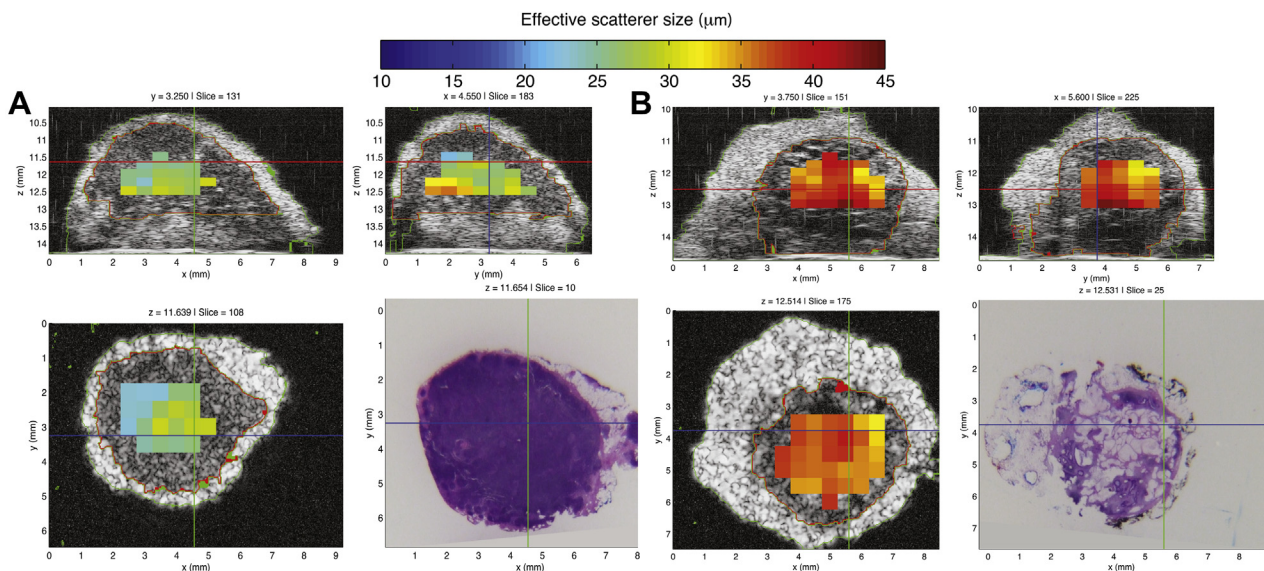


Fig. 3 – Illustrative QUS images: 3D cross-sectional parametric images displaying effective scatter-size estimates. (A) 3D cross-sectional parametric images of a benign locoregional LN from a gastric cancer patient. (3-B) 3D cross-sectional parametric images of a locoregional LN with diffusely metastatic adenocarcinoma from a different gastric cancer patient. Parametric cross-sectional B-mode images are shown with overlaid color-coded effective scatter-size estimates. Bottom right panel of each figure displays the co-registered histology of the bottom left panel. (Color version of figure is available online.)

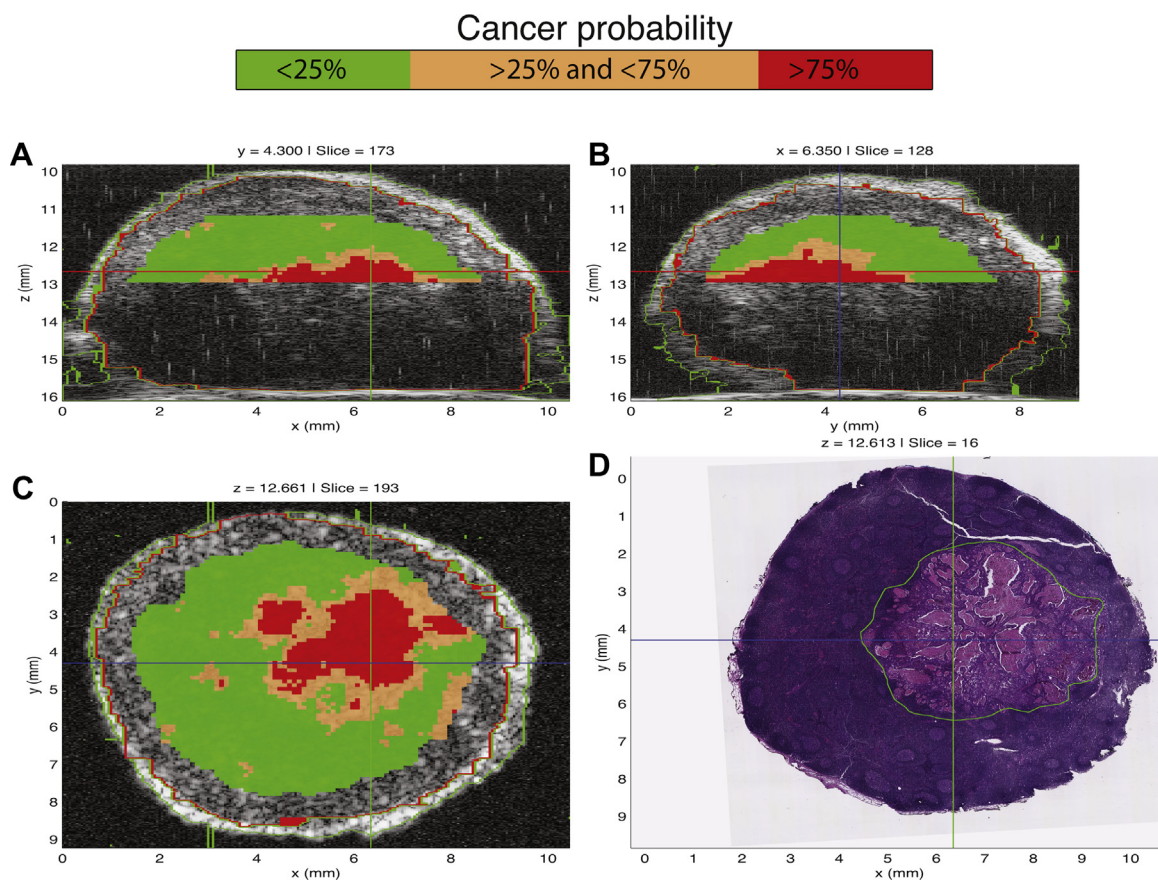


Fig. 4 – 3D interactive GUI with cancer probability images of a locoregional LN with partially metastatic adenocarcinoma from a patient with colorectal cancer. The LN is 9.54 mm at its largest dimension, and the metastasis is 5.09 mm at its largest dimension. The GUI displays three orthogonal grayscale B-mode cross-sections from a 3D rendering in 4A through 4C. The cross sections depict color-encoded cancer probability values, using red to indicate a probability > 75%, orange a probability between 25% and 75%, and green a probability < 25%. Figure 4D shows a co-registered H&E-stained histology photomicrograph corresponding to the same section as in 4C. These images show that excellent concurrence is achieved between the red cancer probability region and the definitive histology result in 4D showing the demarcated metastatic tumor. (Color version of figure is available online.)

2.4. Histology processing

Immediately after ultrasound data acquisition, we inked individual dissected LNs to retain orientation for subsequent reconstruction of node histology in 3D and 3D correlations with QUS results. We bisected inked nodes and then fixed them in 10% formalin for at least 6 h, followed by paraffin processing. We then embedded nodes into paraffin block cassettes. We used a step-sectioning procedure and cut 3- μ m-thin sections at 50- μ m steps from each paraffin block, then stained them with H&E. Two pathologists examined all slides microscopically.

Finally, we obtained fine-resolution (0.23- μ m/pixel) digital photomicrographs of the slides using a virtual digital microscopy scanner (NanoZoomer 2.0-HT; Hamamatsu, Hamamatsu City, Japan). We demarcated metastatic regions using Hamamatsu digital editing software. We performed 3D histology reconstruction and compared 3D histology with 3D QUS images to train and evaluate the classifier, and to verify results.

2.5. Quantitative ultrasound parameter estimation

In this blinded study, an investigator at Riverside Research (New York, NY) analyzed the acquired ultrasound data; the investigator was blinded to the histology results obtained at the Kuakini Medical Center in Hawaii. After all analyses were completed, we compared the QUS and histology results. As described previously [38,39], we estimated QUS parameters based on spectrum analysis and envelope statistics from the acquired RF echo-signal data. These QUS methods are only briefly summarized here.

After image segmentation to separate saline and perinodal fibroadipose tissue from the nodal region, we analyzed acquired RF echo-signal data using a series of overlapping 3D cylindrical regions of interest (ROIs) that were 1 mm long and 1 mm in diameter. We computed an average power spectrum normalized to a water–oil interface from the echo signals in the ROI to obtain four spectrum-analysis–based QUS estimates. A straight-line scattering model provided the spectral slope and spectral intercept [38]. A spherical Gaussian

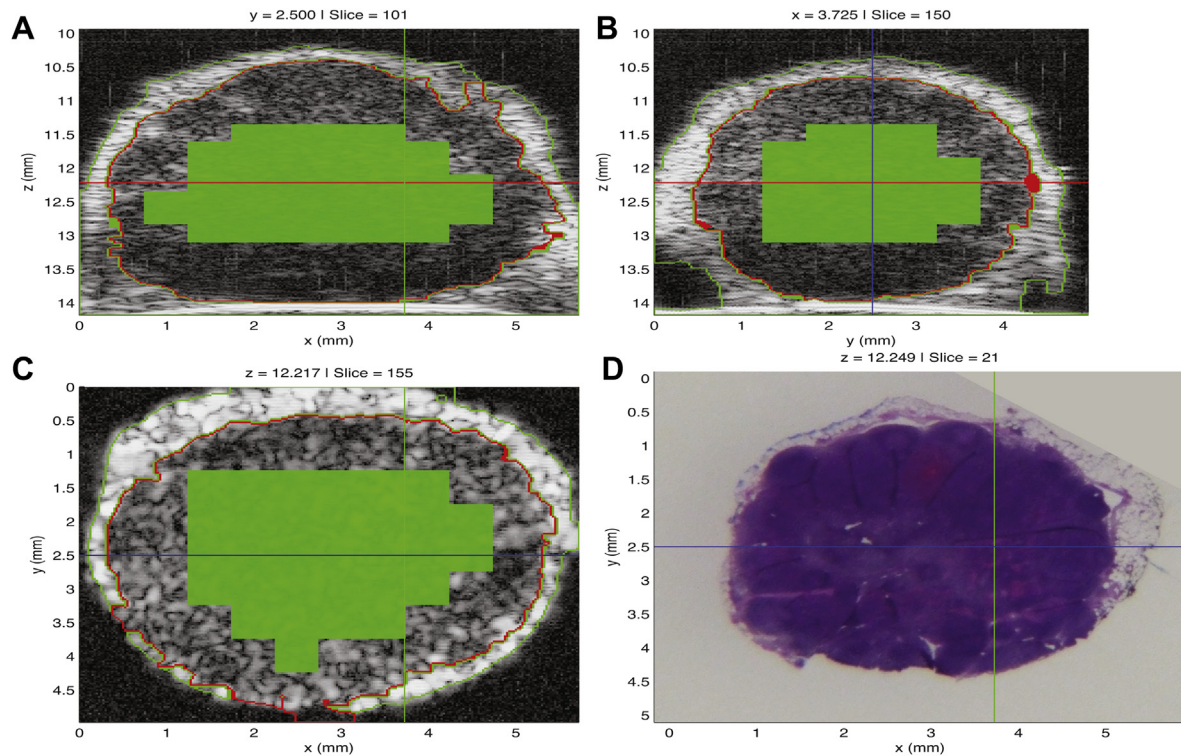


Fig. 5 – 3D interactive GUI with cancer probability images of a benign locoregional LN from a patient with colorectal cancer. The LN is 4.41 mm at its largest dimension. The GUI displays three orthogonal grayscale B-mode cross-sections from a 3D rendering in 5A through 5C. Figure 5D shows a co-registered H&E-stained histology photomicrograph that corresponds to the same section shown in 5C. The cross-sections depict color-encoded cancer probability values, using red to indicate a probability > 75%, orange a probability between 25% and 75%, and green a probability < 25%. These images show that excellent concurrence is achieved between the green cancer probability region and the definitive histology result of the benign LN shown in 5D. (Color version of figure is available online.)

scattering model provided the effective scatter size and acoustic concentration [38].

We computed the envelopes of the RF signals within each ROI; analyses of probability-density functions of the envelope signals provided the four additional QUS estimates. Analyses included application of Nakagami and Homodyned-K statistics models to the envelope signals to derive Nakagami α and Nakagami ω from the Nakagami distribution, and Homodyned-K μ and Homodyned-K k from the Homodyned-K distribution [39]. Finally, we obtained the remaining five QUS estimates using a modified quantile-quantile plot. These estimates were the coordinates of the intersection of low-amplitude and high-amplitude regressions (C_x and C_y) and three slopes estimates (S_l , S_h , and S_a), and were obtained by fitting two regression curves to the modified quantile-quantile plot. These five quantile-quantile estimates quantified the difference between the probability-density functions of the ROI and the Rayleigh-distribution probability-density functions [40].

2.6. Classification

We used all QUS estimates and histologic examination results to classify cancerous and noncancerous LNs using linear-discriminant analysis. Linear-discriminant analysis combined the 13 different QUS estimates to maximize the

differentiation between benign and metastatic tissue in cancer-free and cancer-filled LNs using 50- μ m step-sectioning histology as the reference standard. In addition, we implemented a stepwise approach to remove QUS estimates from linear-discriminant analysis when they did not significantly contribute to classification performance.

Histologic differences between LNs of colorectal and gastric cancer patients compared with LNs of breast cancer patients affect the associated QUS estimates for each type of LN metastasis. Consequently, we obtained distinct classifiers for LNs of colorectal and gastric versus breast cancer, rather than across the entire sample population. Classifier quality was expressed as the area under a receiver-operator characteristics (ROCs) curve (A_z). The A_z values provided quantitative comparisons of classifier performance for different combinations of QUS estimates.

We developed an interactive graphical user interface (GUI) to permit virtual 3D dissection and exploration of freshly dissected LNs; the GUI displays linked, orthogonal, mouse-selected, cross-sectional views of the node with a histology plane that matches the XY ultrasound plane. The interactive display consisted of a grayscale B-mode plane of the 3D volume with overlaid color-encoded QUS estimate or cancer probability values. We estimated cancer probabilities using a Bayesian approach based on the discriminant score, which we described in detail in our previous study [41].

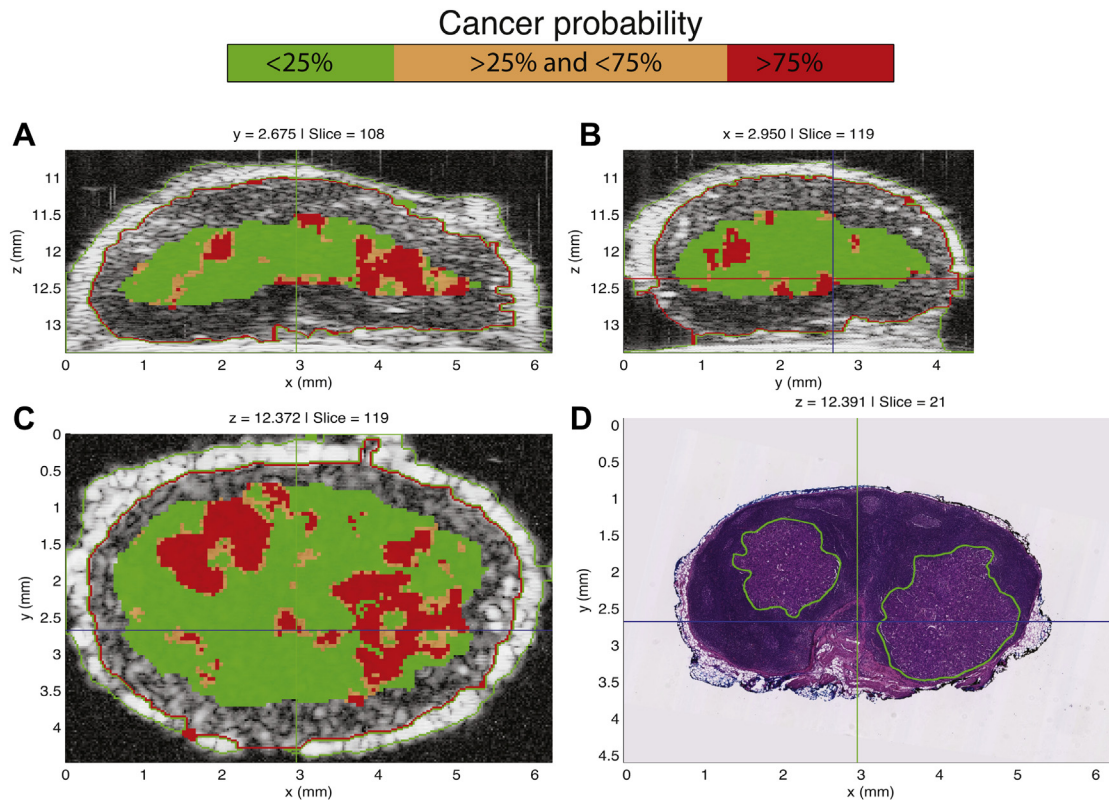


Fig. 6 – Cancer probability images of an axillary LN of a patient with invasive ductal breast cancer. The LN is 5.86 mm at its largest dimension, and it contains two micrometastatic foci. The bigger focus is 1.82 mm at its largest dimension. The GUI displays three orthogonal grayscale B-mode cross-sections from a 3D rendering in 6A through 6C. Cross-sections depict color-encoded cancer probability values, using red to indicate a probability > 75%, orange a probability between 25% and 75%, and green a probability < 25%. Figure 6D shows a co-registered H&E-stained histology photomicrograph that corresponds to the same section shown in 6C. Like Figure 4, Figure 6 shows excellent concurrence between the red high-probability region and the corresponding metastatic region in the histology result. (Color version of figure is available online.)

3. Results

3.1. Classification performance

The Table shows Az values for classification of 290 LNs from 160 patients based on linear-discriminant analysis of the QUS-estimate values. The table also indicates the type of primary cancer and the QUS estimates used as classifiers for each Az value.

Figure 1 displays the ROC curves for LNs of the three cancer types. The ROC curves made the superior classification performance for colorectal and gastric cancers compared with breast cancer readily apparent.

Of 146 LNs of colorectal cancer patients, 23 were metastatic. As shown in Figure 1, linear-discriminant analysis gave an Az of 0.952 ± 0.021 (95% confidence interval [CI]: 0.911–0.993) and sensitivity of 91.3% (corresponding specificity, 87.0%). Of 26 LNs of gastric cancer patients, five were metastatic; linear-discriminant analysis gave an Az of 0.962 ± 0.039 (95% CI: 0.807–1.000). Of 118 LNs of breast cancer patients, 17 were metastatic; linear-discriminant analysis gave an Az of 0.833 ± 0.047 (95% CI: 0.741–0.926) and sensitivity of 88.2% (corresponding specificity, 62.5%). As indicated by the Az values, excellent classification was achieved for LNs

of colorectal cancer and gastric cancer patients. The total number of LNs analyzed for gastric cancer is less than the number of LNs analyzed for colorectal cancer and breast cancer. The classification performance of LNs of colorectal cancer patients was superior to the classification achieved for axillary LNs of breast cancer patients; however, the breast cancer classification results were still satisfactory.

3.2. Illustrative QUS images

Figures 2 and 3 show examples of QUS information expressed as 3D images of QUS-estimate values. These figures respectively illustrate QUS-estimate images of representative benign LNs and diffusely metastatic LNs of colorectal and gastric cancer patients. Segmentation results are color-encoded in green and red. The figures show parametric cross-sectional images displaying effective scatter-size estimates in three orthogonal planes within the 3D volume. The H&E-stained histology shown in the lower right corresponds to the scatter-size image plane shown in the lower left.

Average effective scatter-size estimates were $22.96 \mu\text{m}$ for the benign LN shown in Figure 2A and $33.36 \mu\text{m}$ for the metastatic LN in Figure 2B. Comparison of the two bottom panels of Figure 2A and 2B shows that these illustrative QUS

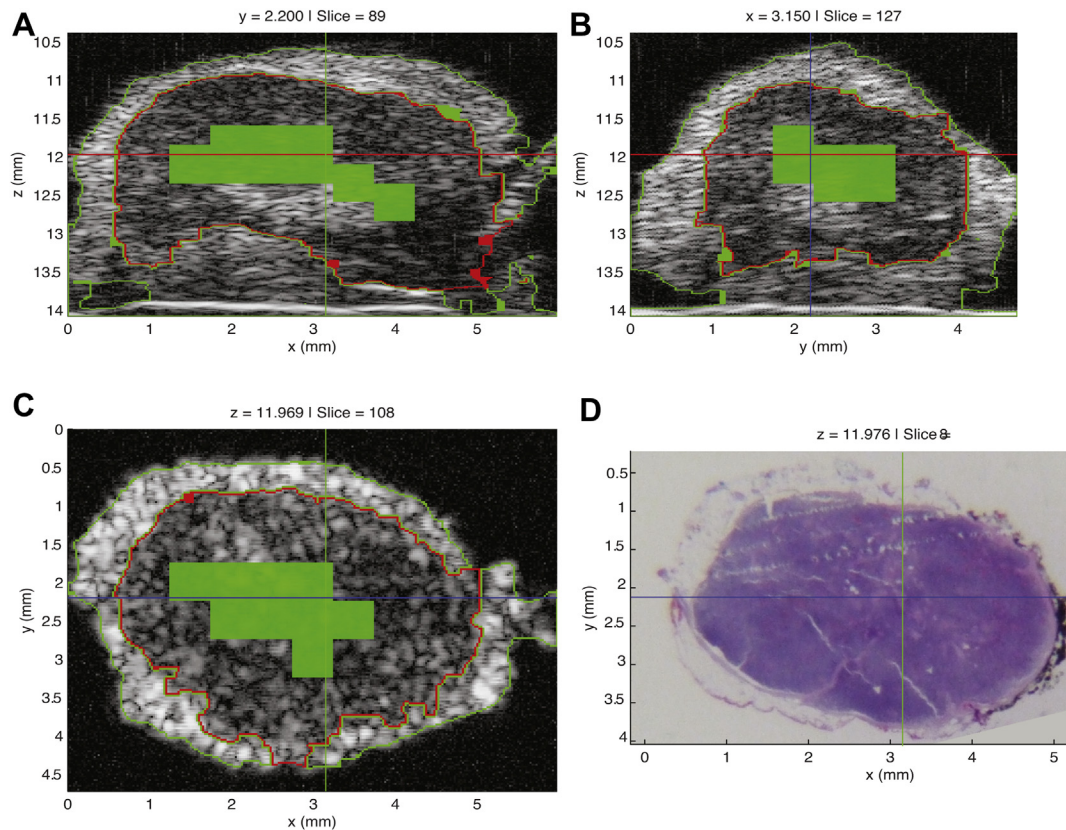


Fig. 7 – Cancer probability images of a benign axillary sentinel LN of a patient with invasive ductal breast cancer. The LN is 5.51 mm at its largest dimension. Cross-sections depict color-encoded cancer probability values, using red to indicate a probability > 75%, orange a probability between 25% and 75%, and green a probability < 25%. Like Figure 5, Figure 7 shows that excellent concurrence is achieved between the green cancer probability region and the definitive histology result of the benign LN shown in 7D. (Color version of figure is available online.)

images suggest that larger effective scatter size may reliably indicate metastases in LNs of colon cancer patients.

Average effective scatter-size estimates were 28.69 μm for the benign LN shown in Figure 3A and 36.69 μm for the metastatic LN in Figure 3B. Comparison of the two bottom panels of Figure 3A and 3B shows that these illustrative QUS images suggest that larger scatter size may reliably indicate metastases in LNs of gastric cancer patients.

For LNs of colorectal and gastric cancers, metastatic LNs displayed larger scatter-size values than cancer-free LNs. These illustrative results suggest that larger scatter size may reliably indicate metastases in LNs of patients with colorectal cancer and gastric cancer. This shows how even a single QUS estimate alone, scatter-size, could aid in identifying suspicious regions.

3.3. 3D interactive GUI with cancer probability images and depiction of micrometastases

A custom GUI displayed 3D QUS and matching 3D histology images for virtual LN interactive evaluation. Figures 4 and 6 show screen captures from this GUI for a partially metastatic LN from a colorectal cancer patient and an LN from a breast cancer patient with micrometastases, respectively. Figures 5 and 7 show screen captures from this GUI for a benign LN

from a colorectal cancer patient and a benign LN from a breast cancer patient, respectively. The GUI displays three conventional B-mode ultrasound images from orthogonal planes X, Y, and Z augmented with overlaid color-coded cancer probability images. The lower right image displays the co-registered XY-plane histology with green outlining cancerous regions indicated in Figures 4 and 6. Comparisons of the XY-plane QUS cancer probability B-mode image with the histology image shows an excellent match between the QUS-based depiction of cancerous regions and the histologically determined micrometastatic and macrometastatic foci. In contrast to Figures 4 and 6, Figures 5 and 7 illustrate how the region classified by QUS-based depiction of cancer probability of <25% matches the histologically proven benign regions.

4. Discussion

4.1. Evolution of metastases detection in LNs using HF-QUS methods

Conventional, clinical, B-mode ultrasound images (<15 MHz) are qualitative and operator and system dependent. Because QUS processing exploits information present in the RF echo signals that is discarded by conventional ultrasound image

processing, QUS methods are sensitive to the microstructural features of tissue that cannot be assessed using conventional imaging methods. The theoretical framework for QUS originally was developed in the 1980s [42]. Since then, QUS approaches for tissue characterization have been extended and refined [38,39,43–58]. In this study, we used HF-QUS (>15 MHz) to ensure sensitivity to small features of tissue micro-architecture on the scale of tens of micrometers. Despite limitations in penetration depth imposed on HF-QUS by frequency-dependent attenuation, the small sizes of the great majority of clinically encountered LNs make HF-QUS applicable for guiding pathologists to suspicious regions in dissected LNs. Furthermore, in this study, we carefully removed excess perinodal adipose tissue during the lymph node retrieval procedure, leaving 0.3–0.5 mm of the surrounding fat layer. In addition to minimizing the attenuation issue, this approach ensured that the entire nodal volume was adequately sampled for entire-volume histology processing. Although we removed the excess perinodal fat layer for this study, we believe that we can better address attenuation concerns once a dedicated system is developed (e.g., by optimizing transmitted power and frequency to increase the penetration depth). In an optimized system, the proposed QUS methods may be potentially applicable to freshly excised surgical specimens, such as colectomy specimens and breast axillary lymph node dissection specimens, before the LN harvest performed by pathologists.

During the early stages of our present study, our group described the basis for 3D HF-QUS methods of LN tissue characterization [38]. Previous studies using linear-discriminant analysis demonstrated that just two of the 13 QUS estimates, effective scatter size and the k parameter using the Homodyned-K distribution, were sufficient to reliably distinguish cancerous from cancer-free LNs of patients with colorectal cancer and gastric cancer. By using these two QUS classifiers alone, 95.0% sensitivity was achieved with 95.7% specificity [39].

Our latest results suggest that HF-QUS methods can reliably identify regions of LNs that are suspicious for LN metastases of all three cancer types investigated. Identification of suspicious LNs was successful not only for diffusely metastatic LNs, but also for LNs with micrometastases.

In our previous studies, all colorectal and gastric cancer patients enrolled had adenocarcinomas. LNs of both colorectal and gastric cancer patients were analyzed together because of the histologic similarity between these types of LNs and the small number of enrolled gastric cancer patients [39]. Metastatic colorectal cancer and gastric cancer in LNs had larger QUS effective scatter size compared with benign LNs. In general, tumor cells are larger than lymphocytes. This may explain the larger QUS estimate of effective scatter size observed in metastatic LNs of colorectal and gastric cancer patients compared with benign LNs. The LN metastases of other cancers are known to have different microscale morphology; for example, LNs of breast cancer patients often present with fatty ingrowths. The variability of axillary LN morphology is well known, and attenuation through the fatty ingrowth in axillary LNs of breast cancer patients, compared with LNs of colorectal cancer patients, may degrade QUS-based classification. This suggests that different QUS

estimate combinations may be more effective for detecting regions suspicious for metastases for different types of primary tumors.

4.2. Interactive 3D cancer probability images as a future pathology tool

Interactive 3D cancer probability images based on HF ultrasound can be made into a small, low-cost pathology tool that can scan LNs immediately after the surgical specimen is received in the pathology laboratory. In this study, we used a custom research scanning system. The scanning time varied between 5 and 30 min, depending on the size of the LN. However, once this method is incorporated into a dedicated system with much faster motors, we believe that the scanning time can be shortened to <2 min/LN for an entire-volume 3D nodal examination.

This will provide a fast, reliable, and operator-independent technique that can scan fresh LNs and provide interactive, real-time, B-mode, ultrasound images with color-encoded cancer probability overlays, as shown in Figures 4, 5, 6 and 7. The LNs also can be scanned intraoperatively immediately after lymphadenectomy or excision of the surgical specimen while the specimen remains intact. This may benefit cancer management by aiding decisions that depend on LN status (e.g., on the number of total metastatic LNs). This tool may assist in detecting small metastatic foci that would be missed by standard, intraoperative, touch-prep or frozen-section procedures, which is especially important for breast cancer sentinel LN biopsy. If QUS-based cancer probability images show regions that are highly suspicious for metastases (e.g., regions with a cancer probability of >75%), the pathologist can target the intraoperative touch-prep procedure or frozen-section procedure to those highly suspicious regions. Also, the operator would be able to adjust the sensitivity and specificity to establish a preferred threshold for decision choices (e.g., to obtain 100% sensitivity with the corresponding specificity). The first potential use for this novel tool would be to guide pathologists to suspicious regions of LNs for definitive histology; if successful, it potentially can dramatically improve detection sensitivity to small metastatic foci that would be missed using conventional histology methods.

This study was limited by the relatively low enrollment of gastric cancer patients, compared with colorectal cancer patients. Future enrollment of additional gastric cancer patients may confirm results obtained to date with LNs of colorectal cancer patients. The total number of LNs acquired per enrolled cancer patient also limited the study. We selected only freshly excised LNs, which excluded LNs harvested after formalin fixation or exposure to fat-dissolving solutions. To avoid delay in diagnosis, which may interfere with the standard of care, we limited the number of LNs processed using our full-volume step-sectioning. As a prospective study, we precluded selection bias by sequentially enrolling patients, randomly selecting LNs for the study from the full surgical specimen, and blinding the investigator who selected the LNs from the specimen to clinical information.

In addition to continuing data acquisition and improving the QUS methods, additional studies are being planned to apply these QUS methods to lower ultrasound frequencies, to

assess their applicability to LN evaluations *in situ*. Our group plans to develop a low-cost, interactive, small, pen-type device based on these results that can instantaneously scan LNs and provide cancer probability results within seconds. The *in situ* application is intended to enable surgeons to identify suspicious axillary sentinel LNs of breast cancer patients in the operating room. This potential device will use a lower frequency to avoid frequency-dependent attenuation challenges at higher frequencies, and will also be intended to scan nonsentinel axillary LNs of breast cancer patients. This may contribute to resolving the current controversy over sentinel LN biopsy, and consequently, may contribute to improving surgical treatment and management of breast cancer.

The *ex vivo* application with higher ultrasound frequencies will enable pathologists to identify suspicious LNs of all three cancer types in the pathology lab. The number of regional LN metastases changes the node status of the tumor-node-metastases staging, and therefore affects cancer staging and prognosis in all three cancer types. This future pathology tool may contribute to more sensitive detection of metastases, and thus more accurate tumor-node-metastases staging by targeting the permanent histology section to the suspicious region.

Our results suggest that the described 3D QUS methods can reliably detect metastases in LNs. Furthermore, these techniques may enable detection of the clinically relevant fraction of micrometastases that are missed by conventional single-section histology. The high probability of missed clinically significant metastases is of great concern because detection of all micrometastases is essential for accurate staging and effective treatment.

Acknowledgments

The authors thank Gregory K. Kobayashi, MD, FCAP, Clifford C. Wong, MD, FCAP, Patricia Kim, MD, FCAP, and Conway Fung, MT, at the Department of Pathology, Kuakini Medical Center, Honolulu, Hawaii, for pathology and histology expertise. Emi Saegusa-Beecroft thanks Professor Keisho Marumo, MD, PhD, Department of Orthopedic Surgery, Jikei University School of Medicine, Tokyo, Japan, for his mentorship. Research reported in this publication was supported by the National Institutes of Health under grant CA 100183, awarded to Ernest J. Feleppa, PhD. The content is solely the responsibility of the authors and does not necessarily represent the official views of the National Institutes of Health.

REFERENCES

- [1] Edge SB, Byrd DR, Compton CC, et al. AJCC (American Joint Committee on Cancer) cancer staging manual. 7th ed. New York: Springer-Verlag; 2010. p. 1–12, 117–126, 143–164, 347–376.
- [2] College of American Pathologists. Protocol for the examination of specimens from patients with primary carcinoma of the colon and rectum. Available from: http://www.cap.org/apps/docs/committees/cancer/cancer_protocols/2012/Colon_12protocol_3200.pdf [accessed 20.03.2012].
- [3] College of American Pathologists. Protocol for the examination of specimens from patients with carcinoma of the stomach. Available from: http://www.cap.org/apps/docs/committees/cancer/cancer_protocols/2012/Stomach_12protocol_3200.pdf [accessed 20.03.2012].
- [4] College of American Pathologists. Protocol for the examination of specimens from patients with invasive carcinoma of the breast. Available from: http://www.cap.org/apps/docs/committees/cancer/cancer_protocols/2012/BreastInvasive_12protocol_3100.pdf [accessed 20.03.2012].
- [5] Viale G, Dell'Orto P, Biasi MO, et al. Comparative evaluation of an extensive histopathologic examination and a real-time reverse-transcription-polymerase chain reaction assay for mammaglobin and cytokeratin 19 on axillary sentinel lymph nodes of breast carcinoma patients. *Ann Surg* 2008;247:136.
- [6] Julian TB, Blumencranz P, Deck K, et al. Novel intraoperative molecular test for sentinel lymph node metastases in patients with early-stage breast cancer. *J Clin Oncol* 2008; 26:3338.
- [7] Wallwiener CW, Wallwiener M, Kurth RR, et al. Molecular detection of breast cancer metastasis in sentinel lymph nodes by reverse transcriptase polymerase chain reaction (RT-PCR): identifying, evaluating and establishing multi-marker panels. *Breast Cancer Res Treat* 2011;130:833.
- [8] Nissan A, Jager D, Roystacher M, et al. Multimarker RT-PCR assay for the detection of minimal residual disease in sentinel lymph nodes of breast cancer patients. *Br J Cancer* 2006;94:681.
- [9] Lyman GH, Giuliano AE, Somerfield MR, et al. American Society of Clinical Oncology guideline recommendations for sentinel lymph node biopsy in early-stage breast cancer. *J Clin Oncol* 2005;23:7703.
- [10] National Comprehensive Cancer Network (NCCN) guidelines. Locoregional treatment of primary breast cancer: consensus recommendations from an International Expert Panel. Available from: <http://www.nccn.org> [accessed 20.10.2012].
- [11] Kaufmann M, Morrow M, von Minckwitz G, et al. Locoregional treatment of primary breast cancer: consensus recommendations from an International Expert Panel. *Cancer* 2010;116:1184.
- [12] Cserni G, Bianchi S, Vezzosi V, et al. The value of cytokeratin immunohistochemistry in the evaluation of axillary sentinel lymph nodes in patients with lobular breast carcinoma. *J Clin Pathol* 2006;59:518.
- [13] Weinberg ES, Dickson D, White L, et al. Cytokeratin staining for intraoperative evaluation of sentinel lymph nodes in patients with invasive lobular carcinoma. *Am J Surg* 2004; 188:419.
- [14] Giuliano AE, Hawes D, Ballman KV, et al. Association of occult metastases in sentinel lymph nodes and bone marrow with survival among women with early-stage invasive breast cancer. *JAMA* 2011;306:385.
- [15] de Boer M, van Dijck JA, Bult P, et al. Breast cancer prognosis and occult lymph node metastases, isolated tumor cells, and micrometastases. *J Natl Cancer Inst* 2010;102:410.
- [16] Weaver DL, Le UP, Dupuis SL, et al. Metastasis detection in sentinel lymph nodes: comparison of a limited widely spaced (NSABP protocol B-32) and a comprehensive narrowly spaced paraffin block sectioning strategy. *Am J Surg Pathol* 2009;33:1583.
- [17] Weaver DL, Ashikaga T, Krag DN, et al. Effect of occult metastases on survival in node-negative breast cancer. *N Engl J Med* 2011;364:412.
- [18] Takeshita T, Tsuda H, Moriya T, et al. Clinical implications of occult metastases and isolated tumor cells in sentinel and non-sentinel lymph nodes in early breast cancer patients:

- serial step section analysis with long-term follow-up. *Ann Surg Oncol* 2012;19:1160.
- [19] Hata M, Machi J, Mamou J, et al. Entire-volume serial histological examination for detection of micrometastases in lymph nodes of colorectal cancers. *Pathol Oncol Res* 2011; 17:835.
- [20] Boler DE, Uras C, Ince U, Cabioglu N. Factors predicting the non-sentinel lymph node involvement in breast cancer patients with sentinel lymph node metastases. *Breast* 2012; 21:518.
- [21] Wu Y, Mittendorf EA, Kelten C, et al. Occult axillary lymph node metastases do not have prognostic significance in early stage breast cancer. *Cancer* 2012;118:1507.
- [22] Grabau D, Ryden L, Fernö M, Ingvar C. Analysis of sentinel node biopsy—a single-institution experience supporting the use of serial sectioning and immunohistochemistry for detection of micrometastases by comparing four different histopathological laboratory protocols. *Histopathology* 2011; 59:129.
- [23] Giuliano AE, Dale PS, Turner RR, et al. Improved axillary staging of breast cancer with sentinel lymphadenectomy. *Ann Surg* 1995;222:394.
- [24] Krishnamurthy S, Meric-Bernstam F, Lucci A, et al. A prospective study comparing touch imprint cytology, frozen section analysis, and rapid cytokeratin immunostain for intraoperative evaluation of axillary sentinel lymph nodes in breast cancer. *Cancer* 2009;115:1555.
- [25] Menes TS, Tartter PI, Mizrachi H, et al. Touch preparation or frozen section for intraoperative detection of sentinel lymph node metastases from breast cancer. *Ann Surg Oncol* 2003; 10:1166.
- [26] Vanderveen KA, Ramsamooj R, Bold RJ. A prospective, blinded trial of touch prep analysis versus frozen section for intraoperative evaluation of sentinel lymph nodes in breast cancer. *Ann Surg Oncol* 2008;15:2006.
- [27] Guidroz JA, Johnson MT, Scott-Conner CE, et al. The use of touch preparation for the evaluation of sentinel lymph nodes in breast cancer. *Am J Surg* 2010;199:792.
- [28] van de Vrande S, Meijer J, Rijnders A, Klinkenbijl JH. The value of intraoperative frozen section examination of sentinel lymph nodes in breast cancer. *Eur J Surg Oncol* 2009; 35:276.
- [29] Veronesi U, Paganelli G, Viale G, et al. Sentinel-lymph-node biopsy as a staging procedure in breast cancer: update of a randomised controlled study. *Lancet Oncol* 2006; 7:983.
- [30] Cserni G, Amendoeira I, Apostolikas N, et al. Discrepancies in current practice of pathological evaluation of sentinel lymph nodes in breast cancer. Results of a questionnaire based survey by the European Working Group for Breast Screening Pathology. *J Clin Pathol* 2004;57:695.
- [31] Van Diest PJ, Torrença H, Borgstein PJ, et al. Reliability of intraoperative frozen section and imprint cytological investigation of sentinel lymph nodes in breast cancer. *Histopathology* 1999;35:14.
- [32] Gobardhan PD, Elias SG, Madsen EV, et al. Prognostic value of lymph node micrometastases in breast cancer: a multicenter cohort study. *Ann Surg Oncol* 2011;18:1657.
- [33] Chen SL, Hoehne FM, Giuliano AE. The prognostic significance of micrometastases in breast cancer: a SEER population-based analysis. *Ann Surg Oncol* 2007;14:3378.
- [34] Reed J, Rosman M, Verbanac KM, et al. Prognostic implications of isolated tumor cells and micrometastases in sentinel nodes of patients with invasive breast cancer: 10-year analysis of patients enrolled in the prospective East Carolina University/Anne Arundel Medical Center Sentinel Node Multicenter Study. *J Am Coll Surg* 2009; 208:333.
- [35] Pepels MJ, de Boer M, Bult P. Regional recurrence in breast cancer patients with sentinel node micrometastases and isolated tumor cells. *Ann Surg* 2012;255:116.
- [36] Giuliano AE, Hunt KK, Ballman KV, et al. Axillary dissection vs no axillary dissection in women with invasive breast cancer and sentinel node metastasis: a randomized clinical trial. *JAMA* 2011;305:569.
- [37] Carlson GW, Wood WC. Management of axillary lymph node metastasis in breast cancer: making progress. *JAMA* 2011; 305:606.
- [38] Mamou J, Coron A, Hata M, et al. Three-dimensional high-frequency characterization of cancerous lymph nodes. *Ultrasound Med Biol* 2010;36:361.
- [39] Mamou J, Coron A, Oelze M, et al. Three-dimensional high-frequency backscatter and envelope quantification of cancerous human lymph nodes. *Ultrasound Med Biol* 2011; 37:345.
- [40] Yamaguchi T, Hachiya H. Proposal of a parametric imaging method for quantitative diagnosis of liver fibrosis. *J Med Ultrasonics* 2012;37:155.
- [41] Mamou J, Saegusa-Beecroft E, Coron A, et al. Three-dimensional quantitative ultrasound to guide pathologists towards metastatic foci in lymph nodes. Proceedings of the Annual International Conference of the IEEE EMBS; 2012 August 28-September 1; San Diego, CA; 2012. p. 1114–1117.
- [42] Lizzi FL, Greenebaum M, Feleppa EJ, et al. Theoretical framework for spectrum analysis in ultrasonic tissue characterization. *J Acoust Soc Am* 1983;73:1366.
- [43] Feleppa EJ, Lizzi FL, Coleman DJ, Yaremko MM. Diagnostics spectrum analysis in ophthalmology: a physical perspective. *Ultrasound Med Biol* 1986;12:623.
- [44] Insana MF, Wagner RF, Brown DG, Hall TJ. Describing small-scale structure in random media using pulse-echo ultrasound. *J Acoust Soc Am* 1990;87:179.
- [45] Insana MF, Hall TJ. Parametric ultrasound imaging from backscatter coefficient measurements: image formation and interpretation. *Ultrason Imaging* 1990;12:245.
- [46] Feleppa EJ, Machi J, Noritomi T, et al. Differentiation of metastatic from benign lymph nodes by spectrum analysis in vitro. Proceedings of the 1997 IEEE Ultrasonics Symposium; 1997 October 5-8; Toronto, Canada; 1997. p. 1137–1140.
- [47] Oelze ML, Zachary JF, O'Brien WD Jr. Characterization of tissue microstructure using ultrasonic backscatter: theory and technique for optimization using a Gaussian form factor. *J. Acoust Soc Am* 2002;112:1202.
- [48] Kolios MC, Czarnota GJ, Lee M, et al. Ultrasonic spectral parameter characterization of apoptosis. *Ultrasound Med Biol* 2002;28:589.
- [49] Mamou J, Oelze ML, O'Brien WD Jr, Zachary JF. Identifying ultrasonic scattering sites from three-dimensional impedance maps. *J Acoust Soc Am* 2005;117:413.
- [50] Baddour RE, Sherar MD, Hunt JW, et al. High-frequency ultrasound scattering from microspheres and single cells. *J Acoust Soc Am* 2005;117:934.
- [51] Oelze ML, Zachary JF. Examination of cancer in mouse models using high-frequency quantitative ultrasound. *Ultrasound Med Biol* 2006;32:1639.
- [52] Mamou J, Oelze ML, O'Brien WD Jr, Zachary JF. Extended three-dimensional impedance map methods for identifying ultrasonic scattering sites. *J Acoust Soc Am* 2008; 123:1195.
- [53] Coron J, Mamou J, Hata M, et al. Three-dimensional segmentation of high-frequency ultrasound echo signals from dissected lymph nodes. Proceedings of the 2008 IEEE Ultrasonics Symposium; 2008 November 2-5; Beijing, China; 2008. p. 1370–1373.

-
- [54] Vlad RM, Brand S, Giles A, et al. Quantitative ultrasound characterization of responses to radiotherapy in cancer mouse models. *Clin Cancer Res* 2009;15:2067.
- [55] Vlad RM, Saha RK, Alajez NM. An increase in cellular size variance contributes to the increase in ultrasound backscatter during cell death. *Ultrasound Med Biol* 2010;36:1546.
- [56] Coron A, Mamou J, Saegusa-Beecroft E, et al. Assembling 3D histology volumes from sections of cancerous lymph nodes to match 3D high-frequency quantitative ultrasound images. *Proceedings of the 2010 IEEE Ultrasonics Symposium*; 2010 October 11-14; San Diego, CA; 2010. p. 2368–2371.
- [57] Mamou J, Saegusa-Beecroft E, Coron A, et al. Three-dimensional quantitative high-frequency characterization of freshly-excised human lymph nodes. *Proceedings of the 2011 IEEE Ultrasonic Symposium*; 2011 October 18-21; Orlando, FL; 2011. p. 27–40.
- [58] Lee J, Karshafian R, Papanicolau N. Quantitative ultrasound for the monitoring of novel microbubble and ultrasound radiosensitization. *Ultrasound Med Biol* 2012;38:1212.